Two organic–inorganic hybrid frameworks with helical structures and large cavities constructed from poly(oxomolybdophosphates)†

Zhaomin Hao, Qingsong Dong, Ling Zhang, Yi Zhang and Fang Luo*

Received 13th August 2009, Accepted 24th October 2009
First published as an Advance Article on the web 27th November 2009
DOI: 10.1039/b916687d

Two novel poly(oxomolybdophosphates) have been synthesized hydrothermally and characterized by single-crystal X-ray diffraction, IR spectroscopy, TG analysis, cyclic voltammetry, and magnetic susceptibility. In compound **1**, the bbi ligands form a series of unusual one-dimensional pores with large apertures through the π···π stacking and hydrogen bonding interactions, meanwhile, the right- and left-hand helical chains are constructed from the $Mn[P_4Mo_6]_2$-type secondary building units that are interspersed in the one-dimensional pore. Compound **2** exhibits a three-dimensional open-framework structure with large cavities where the protonated molecules of ethylenediamine and dissociative water molecules are located.

Introduction

Phosphates, due to their wide structural diversities and potential applications in catalysis, sorption, energy storage, optical and magnetic materials, have received considerable interest.[1–6] Synthetic routes based on typical modular bottom-up approaches are very attractive as they give some control over the final topologies of these materials. Considering the pore size distribution in the regime of molecular-sized holes, as well as the thermochemical stability and the reactive sites, the poly(oxomolybdophosphates) have been described as embodying the attributes of "solid state inorganic enzymes".[7] In all poly(oxomolybdophosphates), the compounds constructed from the $\{P_4Mo_6\}$ basic building unit are structurally very diverse and has extensive application prospects. However, the design and synthesis of such compounds remains a challenge.

Lately, the concept of second building units (SBUs) have been widely used for understanding and predicting topologies of structures by Yaghi, Williams, Kitagawa, and co-workers, and it has been proved to be helpful in directing the construction of a given structure.[8–13] The $\{P_4Mo_6\}$ basic building unit also can be further assembled, *via* a transition metal cation in the +2 oxidation state, into filled-sandwich SBUs of the $M[P_4Mo_6]_2$ type.[14] In the reported examples, we noticed that lots of structures had been synthesized with the $M[P_4Mo_6]_2$-type SBUs,[15] but a study on extending it into the helical structure with large cavities had rarely been carried out.

In this paper, we report two novel organic–inorganic hybrid manganese molybdenum(v) phosphates $(H_2bbi)_{3.5}Na_3\{Mn(H_2O)_3[Mn(P_4Mo_6O_{26}(OH)_5)]_2\}\cdot 4.5H_2O$ (**1**) and $(H_2en)_4\{Mn_2(H_2O)_2[Mn(P_4Mo_6O_{26}(OH)_5)_2]\cdot 5H_2O$ (**2**). Compound **1** exhibits a one-dimensional helical structure constructed from $Mn[P_4Mo_6]_2$-type SBUs. To our knowledge, extended framework solids with one-dimensional helical chain that constructed from $\{P_4Mo_6\}$ units have not been reported. In compound **1**, the bbi ligands form a series of one-dimensional pores with large aperture, and the helical chain constructed from $Mn[P_4Mo_6]_2$-type SBUs intersperse in the pores. Compound **2** consists of a $Mn(P_4Mo_6O_{26}(OH)_5)_2$ (denoted as $Mn[P_4Mo_6]_2$) unit, and around this unit, there are 8 Mn atoms that connect with $Mn[P_4Mo_6]_2$ through covalent interactions. Compared with the known examples, the $Mn[P_4Mo_6]_2$-type SBUs in compound **2** reach the maximum coordination number until now. Meanwhile, the 8 Mn atoms bridge the adjacent $Mn[P_4Mo_6]_2$ units into a three-dimensional open-framework structure with large cavities.

Experimental

General characterization

The IR spectrum for compound **1** and **2** (ESI, Fig. S1)† were recorded in KBr in the 4000–400 cm^{-1} region and exhibit complex patterns with bands at 605–968 cm^{-1} ascribed to υ(Mo=O) and υ(Mo–O–Mo). The absorption bands at 1002–1123 cm^{-1} are assigned to υ(P–O). A series of bands in the region 1380–1650 cm^{-1} are characteristic of the organic ligands. The broad band at 3350 or 3430 cm^{-1} is ascribed to H_2O. These results are in accordance with the structural findings.

In order to examine the thermal stability of compounds **1** and **2**, thermal gravimetric (TG) analyses (ESI, Fig. S2)† were studied from 25 to 600 °C. In compound **1**, the TG curve shows that the first weight loss is 4.21% in the temperature range 65–170 °C, corresponding to the loss of water molecules (calculated value of 3.98%). The second weight loss is 19.6% from 240 to 560 °C, ascribed to the release of the bbi ligands (calculated value of 20.07%). Meanwhile, in compound **2**, the TG curve shows that the first weight loss is 4.6% in the temperature range 30–115 °C, corresponding to the loss of the lattice and coordinated water molecules (calculated value of 4.28%), The second weight loss is 7.84% from 160 to 320 °C, ascribed to the release of the en

Key lab of Polyoxometalate Science, Department of Chemistry, Northeast Normal University, Changchun, 130024, People's Republic of China. E-mail: luof746@nenu.edu.cn; Fax: +86-431-88893336

† Electronic supplementary information (ESI) available: IR spectra and TG curves. CCDC reference numbers 737775 (**1**) and 709205 (**2**). For ESI and crystallographic data in CIF or other electronic format see DOI: 10.1039/b916687d

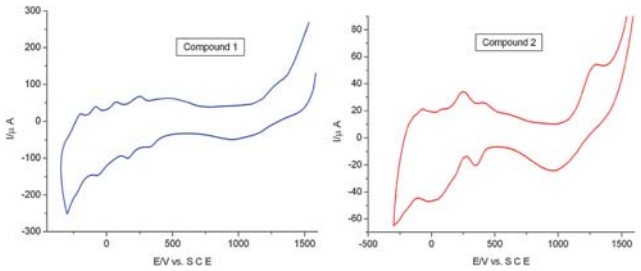

Fig. 1 The cyclic voltammograms of compound **1**-CPE and compound **2**-CPE in 10 mL 0.1M Na_2SO_4 + 8 mL H_2SO_4 aqueous solution at the scan rate of 50 mV s^{-1}.

ligands (calculated value of 8.16%). For compounds **1** and **2**, the final products are a mixture of P_2O_5, $MnMoO_4$, and amorphous material, which are confirmed by PXRD and FTIR studies.

The voltammetric behaviours (Fig. 1) of compounds **1** and **2** are also shown in the 10 mL 0.1M Na_2SO_4 and 8 mL 0.5M H_2SO_4 aqueous solution at the scan rate of 50 mV s^{-1}. The CHI 660 electrochemical workstation connected to a Pentium-IV personal computer was used to control the electrochemical measurements and for data collection. A conventional three-electrode system is used. The working electrode is a glassy carbon; the reference electrode is the Ag/AgCl electrode, and platinum wire is used as a counter electrode. It can be seen that in the range +700 to −200 mV, three redox peaks appear which can be ascribed to the Mo electronic transition. Meanwhile, the peaks in the range +1500 to +800 mV are assigned to the Mn electronic transition.

All reagents were purchased commercially and used without further purification. Deionized water was used for the conventional synthesis. Elemental analyses of carbon, hydrogen and nitrogen were carried out with a PerkinElmer 2400 CHN elemental analyzer.

Synthesis of $(H_2bbi)_{3.5}Na_3\{Mn(H_2O)_3[Mn(P_4Mo_6O_{26}(OH)_5)]_2\}\cdot 4.5H_2O$ (1). (bbi = 1,4-bis(imidazol-l-yl)butane.) A mixture of $(NH_4)_2Mo_7O_{26}$, H_3PO_4, $MnCl_2$, bbi and deionized water in a mole ratio of 1 : 4.3 : 1 : 2.1 : 1150 was stirred for 1 h and then sealed in a 25 mL Teflon-lined stainless steel container. The container was heated to 160 °C and held at that temperature for 72 h, then cooled to 100 °C at a rate of 10 °C h^{-1}, held for 8 h, and further cooled to 30 °C at a rate of 5 °C h^{-1}. A suitable red-brown crystal was selected for structure determination by single-crystal X-ray diffraction. The crystals were easily separated by hand sorting, and the yield of (1) was 33% based on Mn. Anal. calcd: C 12.17, H 2.31, N 5.69. Found: C 12.32, H 2.49, N 5.75.

Synthesis of $(H_2en)_4\{Mn_2(H_2O)_2[Mn(P_4Mo_6O_{26}(OH)_5)_2]\cdot 5H_2O$ (2). The synthesis procedure for compound **2** was identical with that **1**, except the bbi was replaced by en. A red-brown crystal, suitable for single-crystal X-ray studies, was isolated, and the yield of (**2**) was 41% based on Mn. Anal. calcd: C 3.22, H 2.15, N 3.76. Found: C 3.26, H 2.18, N 3.81.

Both compounds **1** and **2** were synthesized with a mixture of $(NH_4)_2Mo_7O_{26}$, H_3PO_4, $MnCl_2$, deionized water, and organic ligands under hydrothermal conditions. In order to determine the influencing factors for the final reaction products, a series of parallel experiments are done. From experience of a large number of experiments, the process of cooling seems to be very important for the result. Following the above of experimental conditions, we got the most and the best of crystals for the characterization of single crystal X-ray diffraction and other properties.

X-Ray data collection and structure determinations

Single-crystal X-ray diffraction data for compounds **1** and **2** were collected on a Bruker Apex CCD diffractometer with graphite-monochromated Mo Kα radiation (λ = 0.71073 Å) at 296 K. Adsorption correction was applied using a multi-scan technique. The structure was solved by direct methods and SHELXL-97[16] and refined by full-matrix least-squares on F^2.[17] During the refinement of **1** and **2**, non-H atoms were anisotropically refined, however, the solvent water molecules in compound **1** was just isotropically refined due to their unreasonable anisotropic U_{eq} parameters and obvious ADP problems. In both compounds, the short $O_{water}\cdots O_{POM}$ distances (2.5–2.8 Å) implied the presence of extensive H-bonding interactions between solvent water molecules and the polyoxoanion. The H atoms on C and N atoms in compounds **1** and **2** were determined in the calculated positions, however, the H atoms on $[H_2PO_4]$ or $[HPO_4]$ groups and water molecules can not be found from the residual peaks and just directly included into the final molecular formula based on the charge-balance consideration. In compound **1**, all positions of Na ions and solvent water molecules were firstly confirmed based

Table 1 Crystal data collection and refinement details for compounds **1** and **2**

	Compound **1**	Compound **2**
Formula	$C_{35}H_{83}Mn_2Mo_{12}N_{14}Na_3O_{69.5}P_8$	$C_8H_{64}Mn_3Mo_{12}N_8O_{69}P_8$
M_r	3390.06	2940.53
Crystal size/mm^3	0.21 × 0.19 × 0.17	0.25 × 0.21 × 0.17
Crystal system	Monoclinic	Monoclinic
Space group	$P2_1/c$	$P2_1/c$
a/Å	14.9478(9)	16.280(11)
b/Å	25.2004(15)	11.924(8)
c/Å	26.7202(13)	18.040(12)
β/°	108.671(3)	103.862(8)
Z	4	2
D_c/g cm^{-3}	2.374	2.872
F(000)	6653	2838
hkl range	$-17 \le h \le 15$ $-29 \le k \le 24$ $-28 \le l \le 31$	$-19 \le h \le 15$ $-11 \le k \le 14$ $-16 \le l \le 21$
θ range/°	1.61 to 25.00	1.93 to 25.50
Reflections collected/unique	48 344/16 773 [R_{int} = 0.0450]	17 681/6330 [R_{int} = 0.0490]
Data/restraints/parameters	16 773/316/1260	6330/16/509
GOF[a] (F^2)	1.017	1.048
R_1, wR_2 [$I > 2\sigma(I)$]	R_1 = 0.0513 wR_2 = 0.1332	R_1 = 0.0387 wR_2 = 0.0994
R_1, wR_2[b] (all data)	R_1 = 0.0784 wR_2 = 0.1499	R_1 = 0.0566 wR_2 = 0.1085
Largest diffraction peak/hole/e Å^{-3}	2.531 and −1.582	1.839 and −1.116
CCDC	737775	709205

[a] GOF = $[\Sigma w(F_o^2 - F_c^2)^2/(n_{obc} - n_{param})]^{1/2}$. [b] $R_1 = \||F_o| - |F_c|\|/\Sigma|F_o|$, w$R_2 = [\Sigma w(F_o^2 - F_c^2)^2/\Sigma w(F_o^2)^2]^{1/2}$.

on the distance references (Na···O > 2.5–2.9 Å, Na···Na > 3.0 Å, O···O > 2.5 Å). Then, their site occupancies were determined as follows: For Na cations, only Na1 is well confirmed and fully occupied. The site occupancies of Na2, Na3, Na4 and Na5 were calculated by fixing their U_{eq} values, which are 1.2 times larger than the one of Na1. The final calculated values are *ca.* 0.60, 0.55, 0.45 and 0.40. Thus, the site occupancies of Na2–Na5 were determined. Following the same method, the site occupancies of disordered solvent water molecules were also confirmed. In compound **2**, the ethylene diamine ion (N3–C4–C3–N4) was refined as a disordered en in two possible positions (N3–C3–C4–N4/N3A–C3A–C4A–N4A) with the occupancies of 50%, respectively. Furthermore, the bond lengths and angles of this en group have been fixed in a reasonable structural model. Moreover, the C4 and C4A possess unusual large U_{eq} values, thus, these U_{eq} parameters have also been fixed with a value 1.2 times larger than those of C3 and C3A, and have just refined isotropically. The detailed crystallographic data and structure refinement parameters for **1** and **2** are summarized in Table 1.

Results and discussion

Structure descriptions of compounds 1 and 2

The structures of **1** and **2** consist of $Mn[P_4Mo_6]_2$-type SBUs. The Mn atom bridges two $\{P_4Mo_6\}$ clusters *via* μ-O atoms, resulting in $Mn[P_4Mo_6]_2$-type SBUs (Fig. 2). As a basic building unit, $\{P_4Mo_6\}$ is a classical metal-oxo cluster and described by Haushalter.[18] In the $\{P_4Mo_6\}$ cluster, it consists of six $\{MoO_6\}$ octahedra and four $\{PO_4\}$ tetrahedra. Each $\{MoO_6\}$ unit has a terminal oxygen and shares edge with neighbouring $\{MoO_6\}$ octahedra. Six $\{MoO_6\}$ octahedra are co-planar and constitute a hexameric molybdenum with alternating Mo–Mo bonds and non-bonding Mo–Mo contacts. Bond valence sum calculation[19] indicate that all Mo and P have +5 oxide state.

$(H_2bbi)_{3.5}Na_3\{Mn(H_2O)_3[Mn(P_4Mo_6O_{26}(OH)_5)]_2\}\cdot 4.5H_2O$ (1). Single-crystal X-ray diffraction analysis reveals that the polymer consists of $Mn[P_4Mo_6]_2$-type SBUs, Na and $Mn(H_2O)_3^{2+}$ cation, protonated bbi ligand, and H_2O solvate molecules. In the polymer, there are two distinct Mn coordination environments. One (Mn1) is located in the $Mn[P_4Mo_6]_2$-type SBUs and displays octahedral MnO_6 coordination geometry with Mn–O bonds at lengths of 2.206 Å × 2, 2.195 Å × 2, 2.213 Å × 2, while the other (Mn2, in form of $Mn(H_2O)_3^{2+}$ cation) is coordinated with six oxygen atoms (O1, O2, O3, O35, O42, O62) from three P–O groups (P3, P7, P8) and two Na–O groups (Na1, Na5) belonging to two different $\{P_4Mo_6\}$ units. Because of the connection of Mn, the $\{P_4Mo_6\}$ units form right- and left-handed helical chains (Fig. 3a and 3b). The chain containing $\{P_4Mo_6\}$ consists alternatively of Mn ions, which have identical configurations along the chain with different orientations. In the polymeric chain, each $\{P_4Mo_6\}$ unit acts as a bidentate ligand coordinating Mn1 or Mn2 through strong Mo–O–Mn or P–O–Mn covalent bond interactions. In this helical chain, each Mn^{2+} cation adopts a six-coordinate approach and act as nodes of the helical chain. The bbi ligands form a large pore (Fig. 3c) with

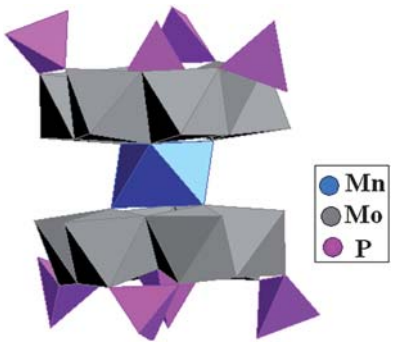

Fig. 2 Polyhedral representation of the $Mn[P_4Mo_6]_2$-type SBU.

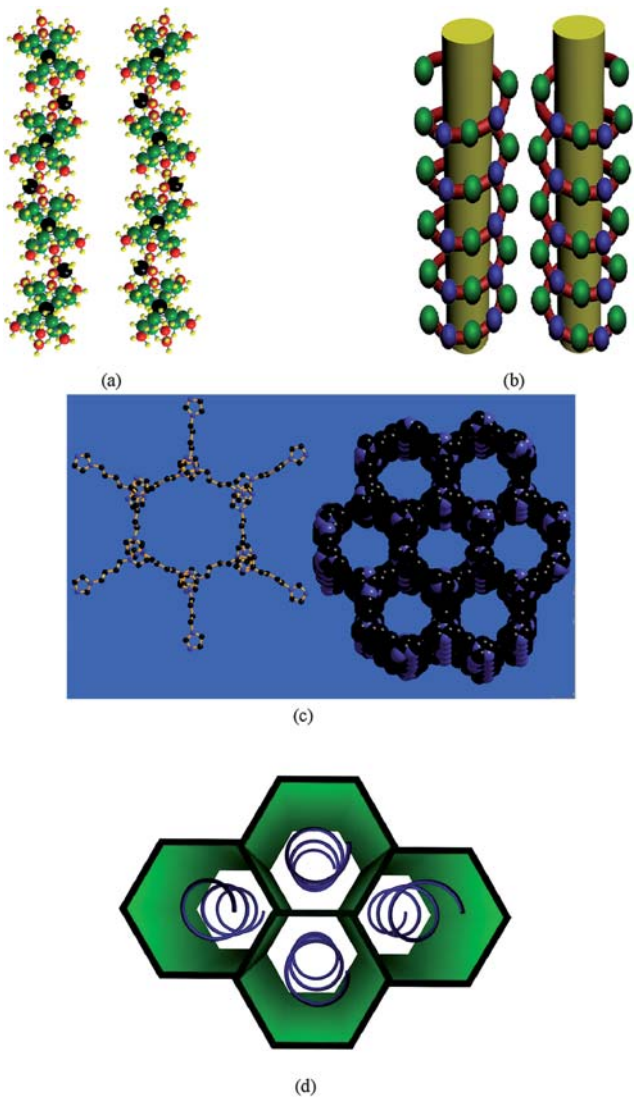

Fig. 3 (a) Detail of the one-dimensional (1D) helical chain constructed from $[Mn(P_4Mo_6)_2]$ unit and manganese (All the hydrogen atoms are omitted; the colour of non-hydrogen atoms: Mo = green; P = red; Mn = black; O = yellow). (b) A schematic illustration of the one-dimensional (1D) helical chain. (The $\{P_4Mo_6\}$ unit is reduced to a green ball, while the Mn atom connected with $\{P_4Mo_6\}$ unit is reduced to a blue ball.) (c) Left, basic unit of the bbi's space-filling diagram; right, space-filling diagram of the bbi ligands. (d) A schematic illustration of the compound **1**.

Table 2 Selected bond lengths (Å) and angles (°) for compound **1**[a]

Bond lengths/Å			
Mn(1)–O(21)	2.195(6)	Mn(1)–O(20)	2.202(6)
Mn(1)–O(15)	2.202(6)	Mn(1)–O(13)	2.203(6)
Mn(1)–O(11)	2.207(6)	Mn(1)–O(14)	2.214(7)
Mn(2)–O(2)	2.242(1)	Mn(2)–O(62)	2.095(8)
Mn(2)–O(35)	2.189(7)	Mn(2)–O(3)	2.224(1)
Mn(2)–O(1)	2.280(9)		

[a] Symmetry codes: (#1) $x, -y-1/2, z+1/2$; (#2) $x, -y-1/2, z-1/2$; (#3) $-x-1, -y, -z-1$.

Bond angles/°			
O(21)–Mn(1)–O(20)	85.1(2)	O(21)–Mn(1)–O(15)	177.5(2)
O(20)–Mn(1)–O(15)	96.2(2)	O(21)–Mn(1)–O(13)	85.3(2)
O(20)–Mn(1)–O(13)	96.5(2)	O(15)–Mn(1)–O(13)	96.7(2)
O(21)–Mn(1)–O(11)	95.2(2)	O(20)–Mn(1)–O(11)	85.6(2)
O(15)–Mn(1)–O(11)	82.7(2)	O(13)–Mn(1)–O(11)	177.9(2)
O(21)–Mn(1)–O(14)	95.7(2)	O(20)–Mn(1)–O(14)	179.1(2)
O(15)–Mn(1)–O(14)	83.0(2)	O(13)–Mn(1)–O(14)	83.3(2)
O(11)–Mn(1)–O(14)	94.6(2)	O(62)–Mn(2)–O(42)$^{\#1}$	170.3(3)
O(62)–Mn(2)–O(35)	107.6(3)	O(42)$^{\#1}$–Mn(2)–O(35)	81.7(3)
O(62)–Mn(2)–O(3)	92.0(4)	O(42)$^{\#1}$–Mn(2)–O(3)	86.4(4)
O(35)–Mn(2)–O(3)	81.6(4)	O(62)–Mn(2)–O(2)	79.7(4)
O(42)$^{\#1}$–Mn(2)–O(2)	91.4(4)	O(35)–Mn(2)–O(2)	169.7(4)
O(3)–Mn(2)–O(2)	105.7(5)	O(62)–Mn(2)–O(1)	97.8(3)
O(42)$^{\#1}$–Mn(2)–O(1)	86.2(3)	O(35)–Mn(2)–O(1)	81.6(3)
O(3)–Mn(2)–O(1)	162.4(4)	O(2)–Mn(2)–O(1)	90.4(4)
Mo(3)–O(11)–Mo(7)	81.8(2)	Mo(3)–O(11)–Mn(1)	134.7(3)
Mo(7)–O(11)–Mn(1)	134.2(3)	Mo(5)–O(13)–Mn(1)	133.5(3)
Mo(1)–O(13)–Mn(1)	133.7(3)	Mo(2)–O(14)–Mn(1)	134.9(3)
Mo(4)–O(14)–Mn(1)	134.3(3)	Mo(9)–O(15)–Mn(1)	133.9(3)
Mo(6)–O(15)–Mn(1)	133.5(3)	Mo(10)–O(20)–Mn(1)	134.2(3)
Mo(11)–O(20)–Mn(1)	133.9(3)	Mo(12)–O(21)–Mn(1)	134.9(3)
Mo(8)–O(21)–Mn(1)	133.6(3)	P(7)–O(35)–Mn(2)	131.9(4)
P(8)–O(42)–Mn(2)$^{\#2}$	148.6(4)	P(3)–O(62)–Mn(2)	49.3(5)

12.4×14.8 Å^2 aperture. The weak π···π stacking and hydrogen bonding interactions between bbi ligands, guarantee the stability of the pore. The one-dimensional helical chain intersperse in the pore (Fig. 3d), and the frame of pore is supported by the one-dimensional helical chain. Adjacent helical chains are linked through Na4 covalent interaction into a 2D sheet, and then the 2D sheets are extended into a 3D network through C···H···O and N···H···O intermolecular forces. The whole 3D supramolecular structure is further stabilized by the hydrogen bonding interaction between lattice water molecule in the framework and the 1D chain. Selected bond lengths and angles for compound **1** are listed in Table 2.

$(H_2en)_4\{Mn_2(H_2O)_2[Mn(P_4Mo_6O_{26}(OH)_5)_2]\cdot 5H_2O$ (2). Single-crystal X-ray diffraction analysis reveals that the polymer includes $Mn[P_4Mo_6]_2$-type SBUs, $Mn_2(H_2O)^{4+}$ cations, protonated en ligands, and H_2O solvate molecules. In compound **2**, around the $Mn(P_4Mo_6O_{26}(OH)_5)_2$ (denoted as $Mn[P_4Mo_6]_2$) unit, there are 8 Mn atoms that connect with $Mn[P_4Mo_6]_2$ through covalent interactions (Fig. 4a). In the polymer, Mn2 displays an octahedral MnO_6 coordination geometry and bridges two $[P_4Mo_6O_{26}(OH)_5]^{7-}$ *via* three μ-O (Mn2–O2, 2.184 Å × 2, Mn2–O3, 2.224 Å × 2, Mn2–O8, 2.224 Å × 2), while Mn1 (in form of $Mn_2(H_2O)^{4+}$) is coordinated by one water molecule (O32) and five oxygen atoms (O5, O9, O24, O27, O28) from four P–O groups (P1, P2, P3, P4) belong to four different $\{P_4Mo_6\}$ unit. The layer stacking along the *a* axis and *b* axis are not aligned to form straight channels, but large cavities (parallelogram windows, with dimensions of 8.38 × 3.25 Å along *a* axis; rhombic windows, with dimensions of 6.95 × 7.28 Å along *b* axis) are created between adjacent layers where the uncoordinated and protonated ethylenediamine cations and dissociative water molecules are located (Fig. 4b and 4c). There are strong hydrogen bonds (ESI, Table S1)† between the open framework and guest molecules. The structure of **2** is stabilized by multi-point hydrogen bonds among $Mn[P_4Mo_6]$ clusters, protonated en and H_2O solvate molecules. Furthermore, from the topological point of view, Mn2 atom as a dual-core unit, is a 6 connection point; meanwhile, the $\{P_4Mo_6\}$ as another node, is also a 6 connection point, so the 3D framework of compound **2** can be abstracted into a $4^{12}6^3$ pcu topology net (Fig. 4d). Selected bond lengths and angles for compound **2** are listed in Table 3.

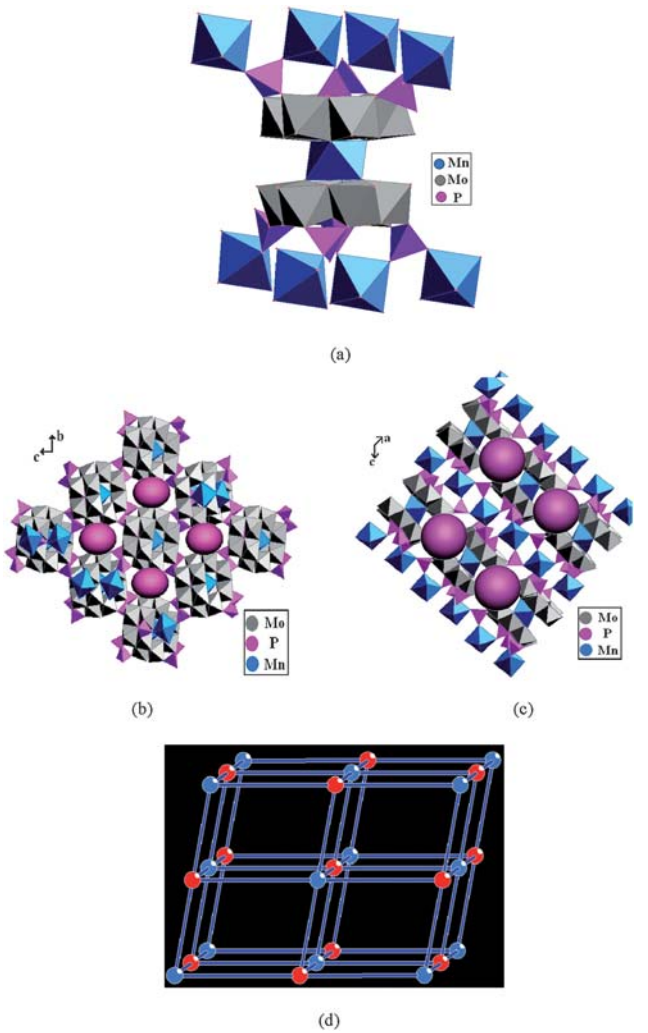

Fig. 4 (a) Polyhedral representation of the basic unit for compound **2**. There are 8 Mn atoms that connect with $Mn[P_4Mo_6]_2$ through covalent interactions, which are shown in blue. (b) The extended structure viewed along the crystallographic *a* axis (without en molecular, and all the cavities are reduced to ellipsoids). (c) The extended structure viewed along the crystallographic *b* axis (without en molecular, and all the cavities are reduced to balls). (d) The topology net of compound **2**.

Table 3 Selected bond lengths (Å) and angles (°) for compound **2**[a]

Bond lengths/Å			
Mn(1)–O(24)	2.098(6)	Mn(1)–O(27)$^{\#1}$	2.141(5)
Mn(1)–O(28)$^{\#2}$	2.157(5)	Mn(1)–O(9)	2.192(5)
Mn(1)–O(32)	2.267(7)	Mn(2)–O(2)	2.184(5)
Mn(2)–O(8)	2.224(5)	Mn(2)–O(3)	2.224(5)
O(5)–Mn(1)$^{\#3}$	2.344(5)		

[a] Symmetry codes: (#1) $-x + 1/2, y - 1/2, -z + 3/2$; (#2) $-x + 1/2, y + 1/2, -z + 3/2$; (#3) $-x + 1, -y + 1, -z + 2$; (#4) $-x, -y + 1, -z + 2$.

Bond angles/°			
O(24)–Mn(1)–O(27)$^{\#1}$	167.3(2)	O(24)–Mn(1)–O(28)$^{\#2}$	99.8(2)
O(27)$^{\#1}$–Mn(1)–O(28)$^{\#2}$	87.4(2)	O(24)–Mn(1)–O(9)	96.5(2)
O(27)$^{\#1}$–Mn(1)–O(9)	94.3(2)	O(28)$^{\#2}$–Mn(1)–O(9)	87.1(2)
O(24)–Mn(1)–O(32)	88.2(2)	O(27)$^{\#1}$–Mn(1)–O(32)	83.4(2)
O(28)$^{\#2}$–Mn(1)–O(32)	168.7(2)	O(9)–Mn(1)–O(32)	99.9(2)
O(24)–Mn(1)–O(5)$^{\#3}$	84.4(2)	O(27)$^{\#1}$–Mn(1)–O(5)$^{\#3}$	86.5(2)
O(28)$^{\#2}$–Mn(1)–O(5)$^{\#3}$	80.81(19)	O(9)–Mn(1)–O(5)$^{\#3}$	167.88(19)
O(32)–Mn(1)–O(5)$^{\#3}$	92.2(2)	O(2)$^{\#4}$–Mn(2)–O(2)	180.00(16)
O(2)$^{\#4}$–Mn(2)–O(8)$^{\#4}$	96.60(18)	O(2)–Mn(2)–O(8)$^{\#4}$	83.40(18)
O(2)$^{\#4}$–Mn(2)–O(8)	83.40(18)	O(2)–Mn(2)–O(8)	96.60(18)
O(8)$^{\#4}$–Mn(2)–O(8)	180.000(1)	O(2)$^{\#4}$–Mn(2)–O(3)	83.44(19)
O(2)–Mn(2)–O(3)	96.56(19)	O(8)$^{\#4}$–Mn(2)–O(3)	83.28(18)
O(8)–Mn(2)–O(3)	96.72(18)	O(2)$^{\#4}$–Mn(2)–O(3)$^{\#4}$	96.56(19)
O(2)–Mn(2)–O(3)$^{\#4}$	83.44(19)	O(8)$^{\#4}$–Mn(2)–O(3)$^{\#4}$	96.72(18)
O(8)–Mn(2)–O(3)$^{\#4}$	83.28(18)	O(3)–Mn(2)–O(3)$^{\#4}$	180.0(3)
Mo(1)–O(2)–Mn(2)	134.4(2)	Mo(3)–O(2)–Mn(2)	134.0(2)
Mo(2)–O(3)–Mn(2)	133.7(2)	Mo(6)–O(3)–Mn(2)	133.3(2)
P(3)–O(5)–Mn(1)$^{\#3}$	146.1(3)	Mo(4)–O(8)–Mn(2)	134.1(2)
Mo(5)–O(8)–Mn(2)	133.2(2)	P(3)–O(24)–Mn(1)	147.3(4)
P(1)–O(9)–Mn(1)	134.3(3)	P(4)–O(27)–Mn(1)$^{\#2}$	141.3(3)
P(2)–O(28)–Mn(1)$^{\#1}$	127.2(3)		

Magnetic properties

The magnetic susceptibility of compounds **1** and **2** were investigated at $H = 0.1$ T and $T = 2.0$–300 K. They are shown in the form of $\chi_m T$ *vs.* T curve, and the $\chi_m{}^{-1}$ *vs.* T curve. In compounds **1** and **2**, Mn^{2+} ($3d^5$; $S = 5/2$) is coordinated by six oxygen atoms from two adjacent $\{P_4Mo_6\}$. Variable-temperature magnetic susceptibility data is obtained on 13.5 mg of a polycrystalline sample of compound **1**. As shown in Fig. 5a, the $\chi_m T$ value is 8.72 emu K mol^{-1} at 300 K, which is slightly smaller than the value of 8.75 emu K mol^{-1} expected for two uncoupled Mn^{2+} ions with $S = 5/2$. The curve fit of $1/\chi_m$ *vs.* T for compound **1** according to the Curie–Weiss law gives $C = 11.28$ cm^3 K mol^{-1} and $\theta = -0.24$ K in the temperature range of 10–300 K, suggesting a weak antiferromagnetic interaction between Mn^{2+} complexes. As the temperature decrease, the $\chi_m T$ value decreases slowly until 50 K and then sharply fall to a minimum value of 5.31 emu K mol^{-1} at 10 K. Below 10 K, the final increase can be attributed to the presence of a small amount of ferromagnetic impurities based on the further susceptibility measurements at different applied field.

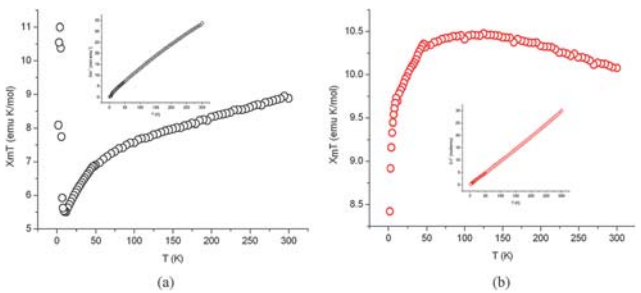

Fig. 5 Magnetic susceptibility measurement results of compounds **1** and **2**.

For compound **2**, the variable-temperature magnetic susceptibility data were obtained on 12.7 mg of a polycrystalline sample of compound **2**. As shown in Fig. 5b, the $\chi_m T$ value is 10.33 emu K mol^{-1} at 300 K, which is smaller than the value for three uncoupled Mn^{2+} ion with $S = 5/2$. According to a known report,[20] the magnetic interactions could be propagated through O–P–O bridges, so these behaviours may be attributed to the interaction of Mn–O–P–O–Mn. As the temperature decrease, the $\chi_m T$ value sharply fall to a minimum value of 8.32 emu K mol^{-1} at 2 K. Such behaviour may result from the zero-field splitting of Mn^{2+} ions.[21,22] Between 50 K and 300 K, the magnetic susceptibility of compound **2** also obeys the Curie–Weiss law [$\chi_m = C/(T - \theta)$] with $C = 4.91$ emu K mol^{-1}. The Weiss temperature $\theta = 0.801$ K shows that weak ferromagnetic interactions exist.

Conclusion

In conclusion, two novel organic-inorganic hybrid manganese molybdenum(v) phosphate has been synthesized by the hydrothermal method. Although a good number of compounds containing $\{P_4Mo_6\}$ unit have been reported, compound **1** is the first example with one-dimensional helical chain that constructed by $Mn[P_4Mo_6]_2$-type SBUs; at the same time, the $Mn[P_4Mo_6]_2$-type SBUs in compound **2** reach the maximum coordination number to date. Linkages of $\{P_4Mo_6\}$ building blocks by other metal cations to form wide structural and potentially applied compound can be envisaged. Further work on this theme is currently under way.

Acknowledgements

We thank the Training Fund of NENU's Scientific Innovation Project (NENU-STC08008) and the Analysis and Testing Foundation of Northeast Normal University

References

1 K. H. Lii, Y. F. Huang, V. Zima, C. Y. Huang, H. M. Lin, Y. C. Jiang and F. L. Liao, *Chem. Mater.*, 1998, **10**, 2599.
2 A. K. Cheetham, G. Ferey and T. Loiseau, *Angew. Chem., Int. Ed.*, 1999, **38**, 3268.
3 X. L. Wang, Y. F. Bi, B. K. Chen, H. Y. Lin and G. C. Liu, *Inorg. Chem.*, 2008, **47**, 2442.
4 S. Y. Song, Y. Zhang, J. Feng, Y. Xing, Y. Q. Lei., W. Q. Fan and H. J. Zhang, *Cryst. Growth Des.*, 2009, **9**, 848.
5 C. Y. Sun, S. X. Liu, D. D. Liang, K. Z. Shao, Y. H. Ren and Z. M. Su, *J. Am. Chem. Soc.*, 2009, **131**, 1883.
6 Carsten Streb, D. L. Long and Leroy Cronin, *CrystEngComm*, 2006, **8**, 629.
7 R. C. Haushalter and L. A. Mundi, *Chem. Mater.*, 1992, **4**, 31.
8 H. L. Li, M. Eddaoudi, M. O'Keeffe and O. M. Yaghi, *Nature*, 1999, **402**, 276.
9 N. L. Rosi, J. Eckert, M. Eddaoudi, D. T. Vodak, J. Kim, M. O'Keeffe and O. M. Yaghi, *Science*, 2003, **300**, 1127.
10 R. Kitaura, K. Seki, G. Akiyama and S. Kitagawa, *Angew. Chem., Int. Ed.*, 2003, **42**, 428.

11 S. S. Y. Chui, S. M. F. Lo, J. P. H. Charmant, A. G. Orpen and I. D. Williams, *Science*, 1999, **283**, 1148.

12 S. M. F. Lo, S. S. Y. Chui, L. Y. Shek, Z. Y. Lin, X. X. Zhang, G. H. Wen and I. D. Williams, *J. Am. Chem. Soc.*, 2000, **122**, 6293.

13 (*a*) P. J. Hagrman, D. Hagrman and J. Zubieta, *Angew. Chem., Int. Ed.*, 1999, **38**, 2638; (*b*) X. H. Bu, W. Chen, S. L. Lu, R. H. Zhang, D. Z. Liao, W. M. Bu, M. Shionoya, F. Brisse and J. Ribas, *Angew. Chem., Int. Ed.*, 2001, **40**, 3201.

14 F. N. Shi, F. A. Almeida Paz, P. I. Girginova, H. I. S. Nogueira., J. Rocha, V. S. Amaral., J. Klinowski and T. Trindale, *J. Solid State Chem.*, 2006, **179**, 1497.

15 (*a*) A. Guesdon, M. M. Borel., A. Leclaire and B. Raveau, *Chem.–Eur. J.*, 1997, **3**, 1797; (*b*) L. Xu, Y. Q Sun, E. B. Wang, E. H. Shen, Z. R. Liu, C. W. Hu, Y. Xing, Y. H. Lin and H. Q. Jia, *J. Solid State Chem.*, 1999, **146**, 533; (*c*) A. Leclaire, A. Guesdon, F. Berrah, M. M. Borel and B. Raveau, *J. Solid State Chem.*, 1999, **145**, 291; (*d*) Y. S. Zhou, L. J. Zhang, X. Z. You and S. Natarajan, *Inorg. Chem. Commun.*, 2001, **4**, 699; (*e*) Y. S. Zhou, L. J. Zhang, X. Z. You and S. Natarajan, *J. Solid State Chem.*, 2001, **159**, 209; (*f*) M. Yuan, E. B. Wang, Y. Lu, Y. G., C. W. Hu, N. H. Hu and H. Q. Jia, *Inorg. Chem. Commun.*, 2002, **5**, 505; (*g*) W. B. Yang., C. Z. Lu, C. D. Wu, S. F. Lu, D. M. Wu and H. H. Zhuang, *J. Cluster Sci.*, 2002, **13**, 43; (*h*) H. X. Guo and S. X. Liu, *Inorg. Chem. Commun.*, 2004, **7**, 1217; (*i*) C. de Peloux, P. Mialane, A. Dolbedq, J. Marrot, F. Varret and F. Sécheresse, *Solid State Sci.*, 2004, **6**, 719; (*j*) H. X. Guo and S. X. Liu, *J. Mol. Struct.*, 2005, **751**, 156; (*k*) H. X. Guo and S. X. Liu, *J. Mol. Struct.*, 2005, **741**, 229; (*l*) W. J. Chang, Y. C. Jiang, S. L. Wang and K. H. Lii, *Inorg. Chem.*, 2006, **45**, 6586; (*m*) Carsten Streb and D. L. Long, *Chem. Commun.*, 2007, 471.

16 G. M. Sheldrick, *SHELXS-97, Program for solution of crystal structures*, University of Göttingen, Germany, 1997.

17 G. M. Sheldrick, *SHELXL-97, Program for refinement of crystal structures*, University of Göttingen, Germany, 1997.

18 R. C. Haushulter and F. W. Lai, *Inorg. Chem.*, 1989, **28**, 2904.

19 I. D. Brown. *Structure and Bonding in Crystals*, Academic Press, New York, 1981, 2, p. 1.

20 Y. S. Ma, R. X. Yuan and L. M. Zheng, *Inorg. Chem. Commun.*, 2009, **12**, 860.

21 E. Coronado, J. R. Galán-Mascarós, C. Giménez-Saiz, C. J. Gómez-García and S. Triki, *J. Am. Chem. Soc.*, 1998, **120**, 4671.

22 X. Z. Liu, G. G. Gao, L. Xu, F. Y. Li, L. Liu, N. Jiang and Y. Y. Yang, *Solid State Sci.*, 2009, **11**, 1433.

